Optically Detected Magnetic Resonance Study of CdS/HgS/CdS Quantum Dot Quantum Wells

E. Lifshitz,* H. Porteanu, and A. Glozman

Department of Chemistry and Solid State Institute, Technion, Haifa 32000, Israel

H. Weller, M. Pflughoefft, and A. Echymüller

Hamburg Universität, Institut für Physikalische Chemie, Bundesstrasse, 45, Hamburg, D-20146, Germany

Received: January 31, 1999; In Final Form: June 10, 1999

CdS/HgS/CdS nanoparticles consist of a CdS core, epitaxially covered by one or two monolayers of HgS, and additional cladding layers of CdS. The luminescence spectrum of the studied materials contains a dominant exciton band located at the HgS layer and an additional nonexcitonic band, presumably corresponding to the recombination of trapped carriers. The present paper describes our efforts to identify the influence of CdS/HgS/CdS interfaces on the localization of the photogenerated species. These properties were investigated by the utilization of optically detected magnetic resonance spectroscopy. The results have shown the existence of two kinds of electron−hole recombination, trapped either at a twin packing of a CdS/HgS interface or at an edge dislocation of an epitaxial HgS or a CdS cladding layer.

Introduction

The nanoparticles of the II−VI, II−V, IV−VI, and III−V semiconductor compounds have been investigated intensively in the past decade.[1−9] These materials exhibit unique chemical and physical properties, differing substantially from those of the corresponding bulk solids. Evidently, these differences are associated with two important characteristics of the nanoparticles: (1) the quantum size effect and (2) the existence of relatively large numbers of atoms at the surface. Moreover, several recent reports have described the development of heteronanoparticles.[10−20] The latter materials are composed of an internal semiconductor core that is coated with several shells of different semiconductors. Examples are the CdS core particle coated with $Cd(OH)_2$,[10] the CdSe core coated with ZnS or CdS,[15] and the HgS core coated with CdS.[17] An interesting form of heteronanoparticles is the onionlike particle, built up by a core of CdS covered by an interior shell of HgS and additional outer cladding layers of CdS. The CdS/HgS/CdS nanoparticles can be synthesized by a wet chemistry method, leading to the formation of tetrahedral[16] shapes. The wide band gap (2.5 eV) of CdS and narrow band gap of β-HgS (0.5 eV) cause a localization of some of the electron and hole states within the HgS internal layer. Therefore, the latter can be viewed as a quantum well and the entire CdS/HgS/CdS structure as a quantum dot quantum well (QDQW). Then, the electron−hole (e−h) excitation and recombination in these structures may be determined by the global confinement of the entire nanoparticle, local confinement in the internal quantum well, and the electron−hole pair interaction. The low-energy exciton transitions have already been measured by absorption, luminescence, fluorescence line narrowing (FLN), and hole burning.[16−21] For example, the absorption spectrum of CdS/HgS/CdS exhibited an absorption onset, red-shifted with respect to bulk CdS, and blue-shifted compared to β-HgS. Initially, the electron, hole, and exciton states were determined theoretically with one-band effective-mass approximation, which was sufficient for the simulation of the low-energy exciton transitions. However, it did not explain the existence of a dark exciton and higher energy transitions. Recently, Bryant et al.[22] have introduced a multiband theory that includes valence-band mixing. The application of this theory suggests that the electron and hole can be trapped either in the same or in different shells. The suggested multiband model at the present time is still lacking a contribution of nonspherical shapes of the particles and pair exchange interactions.

While the excitonic transitions in QDQW samples have been investigated in the past few years, the understanding of the interface's influence on the optical properties has been neglected. Indeed, for particles in such a small regime, a large percentage of the atoms is on/near the internal interfaces or the external surfaces. These sites may act as electron and hole traps. Thus, the present work describes our attempts to clarify the optical properties associated with trapped electrons and holes, utilizing an optically detected magnetic resonance (ODMR) spectroscopy.

Experimental

Material Preparation. The synthesis of the CdS core, with an average size of 5.5 nm, was carried out in a colloidal solution. $Cd(ClO_4)_2$ and H_2S were used as the precursors, while sodium polyphosphate and NaOH acted as a stabilizer and a pH agent, respectively. The core−shell CdS/HgS nanoparticles were prepared by the addition of $Hg(ClO_4)_2$ solution, leading to a displacement of Cd^{2+} ions and the creation of a stoichiometric monolayer (0.3 nm) of HgS. The cladding layer was prepared by a dropwise addition of H_2S/water solution. The reaction with S^{2-} led to reprecipitation of the Cd^{2+} ions over the surface of the particles. The thickening of the HgS layer was simply achieved by repeating the displacement and reprecipitation reactions. The discussed sequence of steps resulted in the formation of the colloidal particles, consisting of a CdS core

* Corresponding author e-mail: ssefrat@tx.technion.ac.il.

10.1021/jp990349c CCC: $18.00
Published on Web 08/06/1999

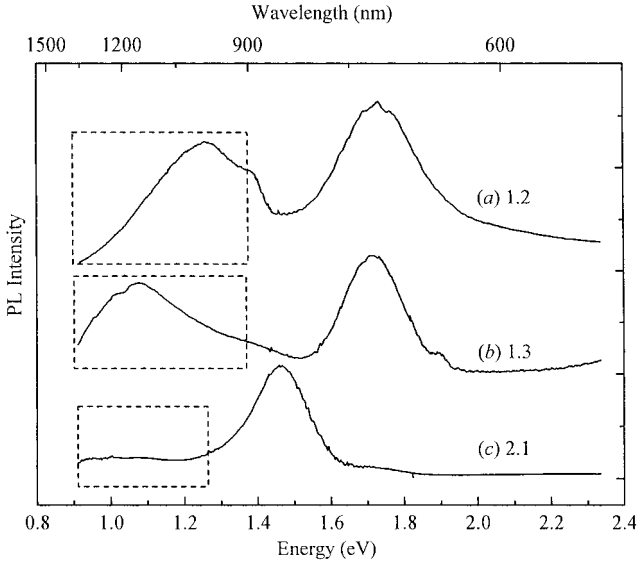

Figure 1. Photoluminescence spectra of QDQW nanoparticles with different thickness of HgS and outer layer CdS.

(cubic, $Eg_{bulk} = 2.5$ eV, lattice parameter $a = 5.818$ Å) surrounded by 1−3 monolayers of β-HgS (cubic, $Eg_{bulk} = 0.5$ eV, $a = 5.851$ Å) and 1−3 outer cladding layers of CdS. A detailed description of the CdS/HgS/CdS nanoparticle synthesis is given in previous publications.[23] The solvents of the QDQW nanoparticle solutions were evaporated and dialyzed with tetrabutyl-amonium hydroxide to purify the particles from the remaining ions and to create an organic surfactant on the external surface. Then the particles could be redissolved in acetone and mixed with a polymer solution. The polymer solution consisted of 6 g of polyvinyl butyral covinyl alcohol in 30 g of acetone. A mixture of the nanoparticles with the polymer, in a 1:1 volume ratio, was stirred at room temperature for 24 h. During this time, most of the excess solvent was evaporated and the polymer hardened gradually. The mixture vessel was covered with paraffin paper to avoid fast evaporation. This prevented the creation of cracks and bubbles within the polymer and ensured the formation of uniform films. The resulting polymer films, embedded with the CdS/HgS/CdS nanoparticles, were utilized for the optical measurements discussed below.

Instrumental. The PL and ODMR measurements were carried out by immersing the samples in a cryogenic dewar (at 1.4 K) and exciting them with continuous 2.71 eV Ar^+, 2.41 eV Ar^+, or 1.90 eV Ti−sapphire laser. The emitted light was passed through a holographic grating monochromator and detected by Si, Ge, or PbS detectors. The ODMR spectra were recorded by placing the sample on a special sample probe at the center of a High-Q resonance cavity, coupled to a microwave (mw) source (∼10 GHz) and surrounded by a superconducting magnet (B). These spectra were obtained by measuring the change in luminescence intensity of the nonexcitonic PL band (framed by the dashed line in Figure 1) induced by an electron spin magnetic resonance event at the excited state. This change was plotted versus the strength of the external magnetic field, *B*, leading to magnetic resonance-like spectra. The nonexcitonic luminescence was isolated by appropriate cutoff color filters, while the emitted beam was detected in either of the following directions: (a) parallel to the external magnetic field (Faraday configuration) or (b) perpendicular to it (Voight configuration). A total emission or a circular-polarization component was detected in the Faraday configuration.

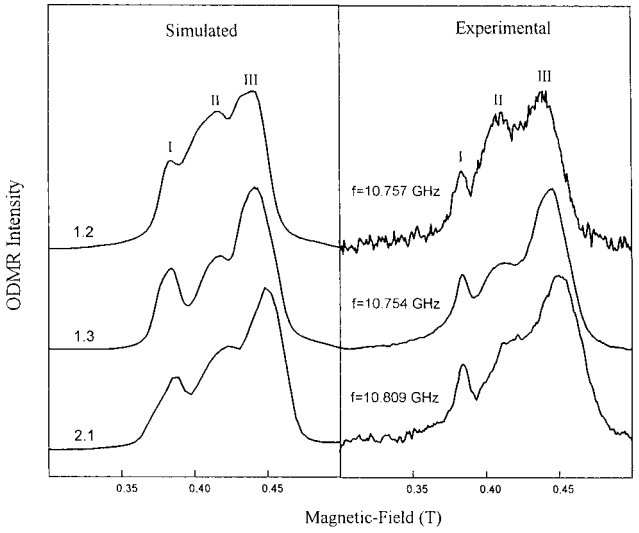

Figure 2. Representative experimental (right) and simulated (left) ODMR spectra of the 1.2, 1.3, and 2.1 samples.

Results

Representative PL spectra of CdS/HgS/CdS samples, excited above the core-CdS band-gap energy and recorded at 1.4 K, are shown in Figure 1(a−c). Figure 1(a) corresponds to a sample with a monolayer of HgS and two outer cladding layers of CdS (labeled 1.2). Figure 1(b) corresponds to a sample with a monolayer of HgS and three CdS cladding layers (labeled 1.3). Figure 1(c) represents a sample with two layers of HgS and a cladding monolayer of CdS (labeled 2.1). The spectra in the figure consist of an exciton band (centered at 1.70 eV), predominantly tunable with the thickness of the internal HgS layer, and an additional broad band at lower energies (centered at 1.10−1.30 eV). The latter is mainly pronounced in the samples with a thin HgS layer (the 1.2 and 1.3 samples). It should be noted that similar PL spectra were obtained with excitation energy below the core band gap (with 2.41 and 1.9 eV), when the latter approaches a resonance excitation of the HgS component (vide infra).

The ODMR method was utilized in order to follow the recombination mechanism of the nonexcitonic luminescence band (framed by the dashed line in Figure 1) and to understand the influence of interface or surface states on this recombination. It should be emphasized that the major part of the exciton spectral regime did not exhibit an ODMR signal, while the low energy tail occasionally presented a weak magnetic resonance signal. However, the nonexcitonic band always produced an intense ODMR spectrum. Experimental spectra of the nonexcitonic regime of the 1.2, 1.3, and 2.1 samples, recorded in the Voight configuration with a laser excitation power of 15 W/cm^2, are shown at the right column of Figure 2. These consist of three magnetic resonance signals (labeled I, II, and III in the figure), ranging between 2000 and 5000 G, with corresponding *g*-factors as given in Table 1. Further explanation regarding the *g*-factor will be given in the next section. Identical ODMR spectra were observed either by 2.71 or by 2.41 eV excitation (above and below the core CdS band gap).

Each one of the ODMR spectra was examined at various experimental conditions. For example, the corresponding spectra of the 1.3 sample, recorded at different microwave output modulation frequencies, are shown in Figure 3. The ODMR spectra of the same sample, recorded with different laser excitation power, are shown in Figure 4. Careful observation of the last two figures suggests that the resonance signals III

TABLE 1: Spin Hamiltonian Parameters of the ODMR Resonance Signals: I, II, III

sample		g_{xx}	g_{yy}	g_{zz}	J (meV)	D (meV)	P (thermal parameter)
1.2							
	peak I	1.87	1.98	1.85	0.004 ± 0.0005	0.002	0.65
	peak II	1.812	2.02	1.812	$\gg g\beta B$	0.001	0
	peak III	1.684	1.764	1.65	0.004 ± 0.0005	0.002	0.65
1.3							
	peak I	1.901	1.961	1.869	0.004 ± 0.0005	0	0.65
	peak II	1.82	2.02	1.83	$\gg g\beta B$	0.002	0
	peak III	1.685	1.742	1.685	0.004 ± 0.0005	0	0.65
2.1							
	peak I	1.87	1.98	1.85	0.004 ± 0.0005	0.002	0.65
	peak II	1.77	1.77	1.77	$\gg g\beta B$	0.001	0
	peak III	1.65	1.73	1.67	0.004 ± 0.0005	0.002	0.65

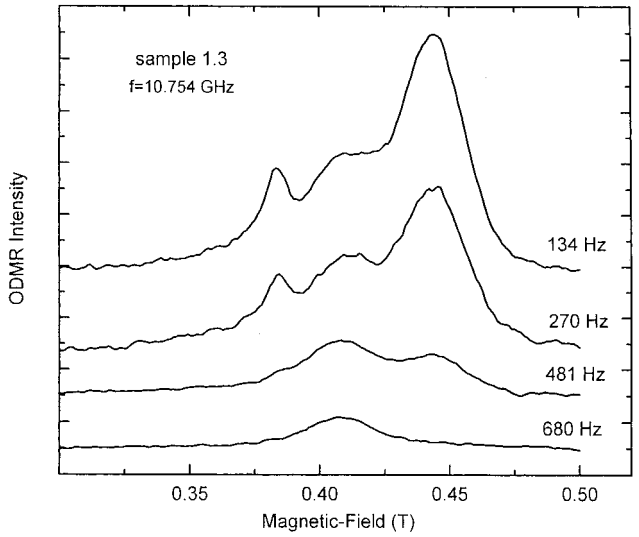

Figure 3. The ODMR spectra of the 1.3 sample, recorded at different microwave output modulation frequencies.

and I alter simultaneously, while resonance II behaves differently. This suggests that the latter spectra consist of two overlapping magnetic resonance events and, more likely, resonance III and I correspond to a common incident. Examination of the microwave modulation frequency and laser power dependence of the ODMR spectra of samples 1.2 and 2.1 shows a similar behavior to that described for the 1.3 sample.

Discussion

The PL spectra shown in Figure 1 contain an exciton band that is red-shifted with respect to the CdS energy band, but blue-shifted with respect to the β-HgS bulk energy band. Moreover, the energy of this exciton is predominately influenced by the thickness of the HgS shell, while this energy is only slightly adjusted by the thickness of the CdS cladding layer or the dimension of the CdS core.[24] Thus, it was previously suggested[16] that the exciton is associated with optical transitions between the lowest quantized energy levels of the HgS quantum well. Further investigation of the exciton region is given elsewhere.[16] However, the nature of the nonexcitonic luminescence will be discussed thoroughly in the following paragraphs by the analysis of the ODMR measurements.

The ODMR spectra of the various QDQW samples, detected at the nonexcitonic band region, consist essentially of the representative resonance signals I, II, and III, as shown in Figure 2. Although resonance I appears slightly narrower than the others, the dependence on the experimental parameters (Figures 3 and 4) suggests that resonance III and I are associated with a

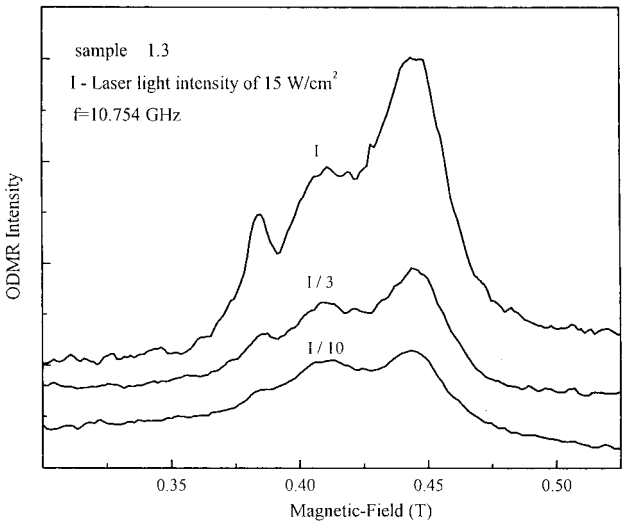

Figure 4. The ODMR spectra of the 1.3 sample, recorded with different laser excitation power.

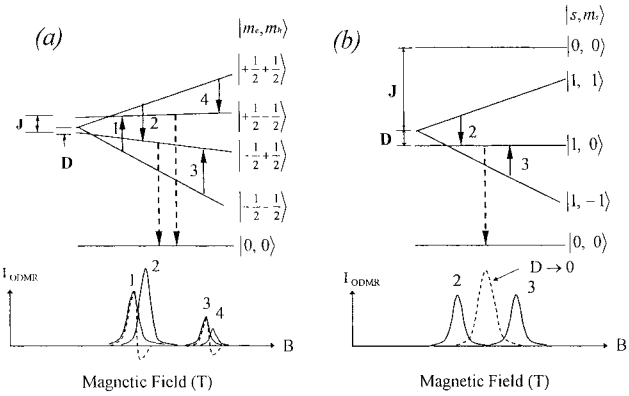

Figure 5. Schematic diagram of the spin energy states of recombining electron and hole. (a) Spin state diagram with weak J (e.g., separate e−h pair). (b) Spin state diagram with strong J (e.g., triplet exciton).

similar incident, while resonance II has an independent behavior. Thus, the ODMR spectra consist of two overlapping electron−hole recombination events. Each one of them can be simulated by the following phenomenological spin Hamiltonian:

$$Hs = \beta S_e g_e B + \beta S_h g_h B + S_e D S_h + J S_e S_h \qquad (1)$$

The first two terms correspond to the effective Zeeman interaction of an electron and hole, the third term corresponds to the zero field splitting (may be overlapped by an anisotropic exchange interaction), while the last term, to the isotropic electron−hole (e−h) exchange interactions. Since the spectra shown in Figure 2 were observed either by Faraday (with and without circular polarization) or Voight configuration detection, we can assume that the magnetic resonance transitions are not associated with a change in angular momentum between excited and ground states. Thus, the excited-state spin manifold corresponds to electron (e) and hole (h) levels, each with an effective spin quantum number of $S = 1/2$ and the corresponding projection along the direction of the external magnetic field of $m_S = \pm 1/2$. The diagrams shown in Figure 5 describe two extreme possibilities of a spin manifold, where the numbers 1−4 show the spin resonance transitions, while the dashed arrows designate the optical transitions. J corresponds to an isotropic e−h exchange interaction, while D to the zero-field splitting. Obviously, the e−h mutual interactions determine the variability of the resonance transitions. For a relatively weak J, the electron

and hole preserve their independent spin quantum number of $S = 1/2$ and form the spin manifold, shown in Figure 5a. The zero-angular momentum optical transitions take place from the $|+1/2, -1/2\rangle$ and $|-1/2,+1/2\rangle$ sublevels. Furthermore, if thermal distribution of the spin states population does not occur, then the magnetic resonance transitions marked by the solid arrows in the figure will enhance the intensity of the optical transitions. The anticipated ODMR spectrum is shown in the lower portion of Figure 5(a,b). It consists of two doublets; each is associated with the flipping of the electron (transitions 1 and 2) and hole (transitions 3 and 4) projection direction. The separation within a doublet corresponds to J, while the separation between the doublets is associated with the individual g-factor of the electron and hole. However, upon thermal distribution among the spin states, some of the resonance transitions may reverse their sign. The latter will lead to a quenching of the optical transitions and the appearance of negative signals in the ODMR spectra (shown by a dashed line in the left-anticipated spectrum).

For $J \gg \beta gB$ (45 μeV), the $|+1/2, -1/2\rangle$ spin state is pushed to a higher energy, creating singlet ($S = 0$) and triplet ($S = 1$) spin states, as shown schematically in Figure 5b. The zero-angular momentum optical transition originates from the triplet $|1,0\rangle$ state and the magnetic resonance transitions 1 and 4 are eliminated. Thus, the anticipated spectrum, drawn below the diagram, consists of resonance signals (2 and 3) corresponding to the transitions among a triplet manifold, with mutual separation which is equal to D. When $D \rightarrow 0$ the ODMR spectrum will coalesce into a single broad resonance, as presented by the dashed line in the corresponding anticipated spectrum.

The Hamiltonian given in eq 1 and the considerations discussed above were utilized in order to simulate each one of the resonance events. The evolution of the simulation is illustrated in Figure 6. Resonance signals III and I resemble a case with a relatively weak exchange interaction. Thus, in the first stage the simulation included small J and D and isotropic g-factor (curve 6a). It consists of a narrow and symmetric resonance signal, in contradiction with the experimental spectra. Incorporation of anisotropy in the g-factor led to an asymmetric broadening in the resonance signals (curve 6b). The last was, more or less, sufficient for the simulation of resonance III. However, it did not predict the narrow appearance of resonance I and the relative intensities between resonance I and III. This could be simulated by an addition of thermalization parameter (curve 6c), which is denoted as a variable P in Table 1 and corresponds to a degree (ranging between 0 and 1) of a Bolzman population distribution among the spin states. As indicated before, such a thermal distribution process results in quenching of a part of the resonance signal and consequently, narrowing of the remaining part of it. The last stage of the simulation included an essential additional broadening, associated with the distribution of J values (curve 6d). The amount of distribution in this parameter is given by the standard deviation in Table 1. As a summary, consideration of anisotropic g, distribution of J values, and thermalization factor all lead to a best fit of resonance I and III, as shown by the solid line in curve 6d.

Observation of resonance II suggests that it is associated with e−h pair recombination with relatively strong isotropic exchange interaction ($J \gg g\beta B$) and $D \ll J$. The small D value leads to coalescence of the resonance into a single band with an average g-factor [$g_{avr} = (g_e + g_h)/2$]. Consideration of anisotropic effects and broadening parameters followed similar evolution as for resonance signals I and III and led to the simulated curve shown in Figure 6e. Then, a summation of curves 6d and 6e gave the best-fit with the experimental spectrum (curve 6f), when the simulated parameters are summarized in Table 1.

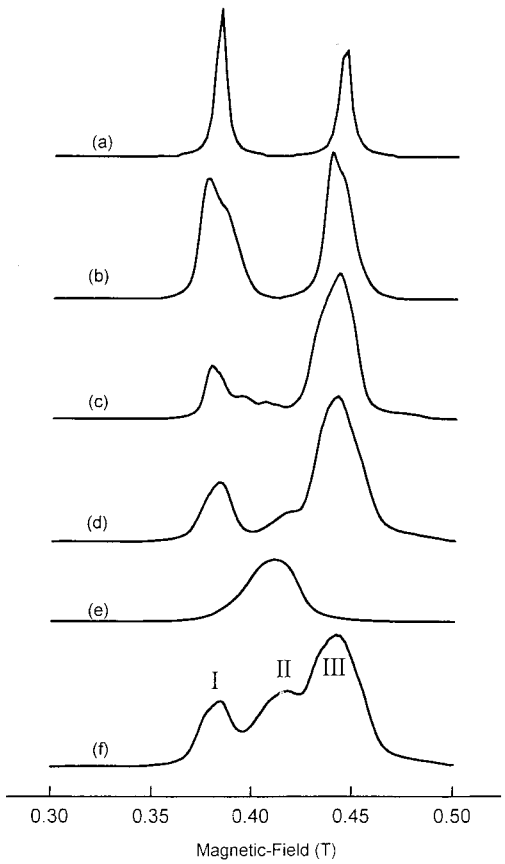

Figure 6. The evolution of the simulation ODMR spectra: (a) isotropic g-factor, J, and $D = 0$; (b) incorporation of anisotropy in the g-factor; (c) incorporation of thermalization parameter; (d) incorporation of the distribution of J values; (e) simulated curve of the resonance II; (f) final simulated curve of the experimental ODMR spectra.

The J values indicated in Table 1, are smaller than the exchange interaction of a typical exciton in II−VI nanoparticles (~0.3 eV in CdSe nanoparticles[25]), supporting the nonexcitonic character of the studied recombination emission. The g values of the different resonance signals range between 1.65 and 2.02. This can be compared with a reported $g = 1.78$ [26,27] of either a shallow donor or the conduction band of CdS bulk or nanoparticles. Thus, the observed values in the present case may be associated with shallow trapping of an electron. However, it deviates substantially from $g = 1.15$, reported for the CdS valence band.[28] Thereupon, the present work corresponds to a recombination between shallow trapped electron state at a CdS interface, with a deep hole-trapping state, deferring from the properties of a CdS band edge.

The PL measurements showed that the nonexcitonic band can be excited below the band-gap energy of CdS, thus suggesting that it is associated with defect states either in the HgS well or at the CdS/HgS interface. This excludes the possibility that this band is associated with surface defects of the CdS cladding layer or within the CdS core. In addition, the ODMR spectra of core CdS particles, capped with similar organic termination, showed completely different resonance signals. The last spectrum and its simulation will be reported elsewhere.

The anisotropy of the trapping sites associated with resonances I and III excludes the possibility of their location at substitutional or interstitial sites within a cubic zinc blende nanoparticle. Instead, it suggests localization at an interface or surface. Several suggestions regarding the chemical nature of

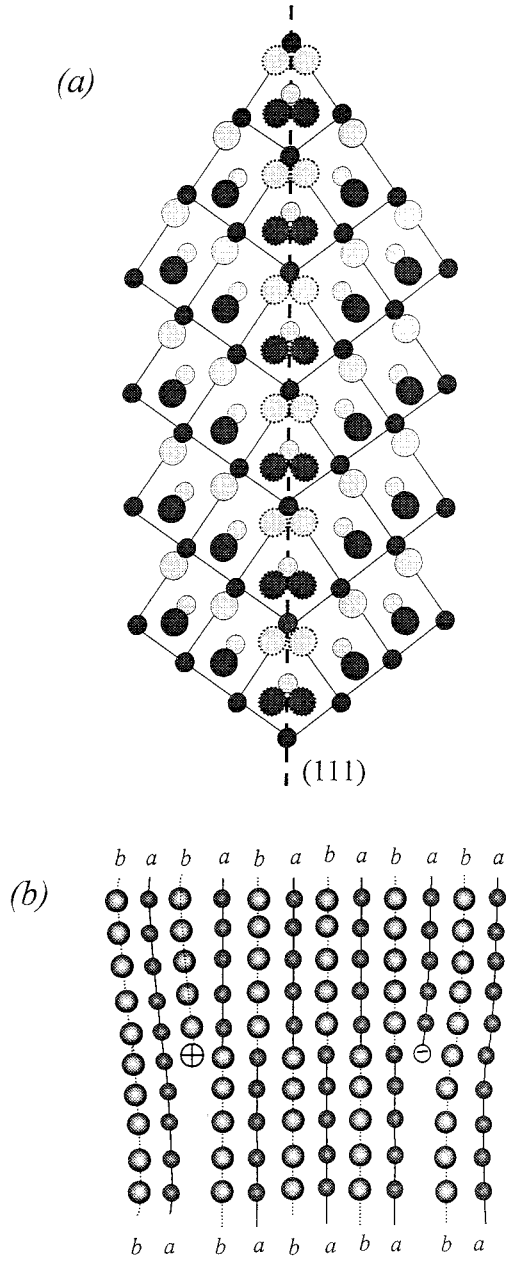

Figure 7. (a) Twin grain boundary in the (1̄11) surface of a cubic AB compounds. Plane of main drawing is (1 1̄ 0); small and large dark circles represent Cd and S in the plane, small and large light circles represent Cd and S in the layers immediately above or below of plane (1 1̄ 0) displaced by $a/[2(2)^{1/2}]$. (b) Particle dislocations in AB compounds. The small circles represent Cd(Hg), the large circles represent S.

the trapping sites can be raised. Mews et al.[16] showed that the crystallization of CdS/HgS/CdS nanoparticles results in tetrahedral shapes with (111) facets. They also indicated the possibility of twin grain boundaries between HgS and the adjacent CdS core and cladding layer. Such a boundary is shown schematically in Figure 7a. It is obviously seen in the last figure that the stacking of the atoms at the boundary is too crowded and therefore, a crystallographic rearrangement will take place. It can include gliding or elimination of some atoms.[29] The latter involves the formation of vacancies either of a metal (Cd, Hg) or of a sulfur. Cd^{2+} and S^0 vacancies act as double acceptors. However, trapping of a single hole alone leads to the creation of paramagnetic centers that can be detected by the ODMR method. Cd^0 and S^{2-} vacancies act as double donors, and, in a similar manner, the trapping of one electron will be detected by the ODMR method. In other words, photogenerated electrons and holes can be trapped at vacancy defects that are created at the twin grain boundaries in QDQW structures. The unique principal axis (the spectroscopic *g*-factor) is considered to be normal to the boundary while the other axes are tangential to it. Accordingly, the distribution of exchange interaction values can be due to the existence of an ensemble of e−h pair distances, more likely, around the periphery of an interface. The twin grain boundaries can very well describe the resonance signals in the ODMR spectra. The occurrence of vacancies at attached sites along the twin boundary leads to trapping of electrons and holes that strongly interact by exchange mechanism and can be associated with resonance signal II. However, larger spatial distribution of trapped electron and hole along the twin boundary may lead to a weaker exchange interaction and to the origin of the I and III resonance signals.

Alternatively, Mews et al. showed that the growth of a monolayer is not perfect[16] and it can be terminated by an edge dislocation, as shown schematically in Figure 7b. In a manner similar to the described vacancies, such terminations have unsaturated chemical bonds, creating electron and hole trapping sites. Likewise, these edges have asymmetric local chemical bonds reflected in an asymmetric *g*-factor. These edge dislocations are distributed randomly and may be spaced apart by more than two-chemical bonds. Thereupon, the exchange interaction of carriers trapped in those sites will be relatively small. Hence, the edge dislocations can be associated with trapped e−h pairs that produce the resonance signals III and I in the studied ODMR spectra.

In conclusion, the optical properties of QDQW are governed by the properties of the CDS/HgS interface. This acts as trapping sites for photogenerated carriers. The exchange between an e−h pair at the interface is smaller than an exciton, reflecting their localization properties. The ODMR methods revealed some knowledge regarding the mechanism of recombination and the identity of the interface sites.

Acknowledgment. This project was supported by the German−Israel science foundation (GIF) contract no. I-0414-021.10/95. H.P. thanks the Israeli Council for Higher Education Postdoctoral Fellowship for support.

References and Notes

(1) Martin, T. P.; Naher, U.; Schaber, H.; Zimmermann, U. *J. Chem. Phys.* **1994**, *100*, 2322.
(2) Bawendi, M. G.; Carrol, P. J.; Wilson, W. L.; Brus, L. E. *J. Chem. Phys.* **1992**, *96*, 946.
(3) Echymüller, A.; Hässelbarth, A.; Katsikas, L.; Weller, H. *Ber. Bunsen-Ges. Phys. Chem.* **1991**, *95* (1), 79.
(4) Henglein, A. *Chem. Rev.* **1989**, *89* (8), 1861.
(5) Wang, Y.; Herron, N. *J. Phys. Chem.* **1987**, *91*, 257.
(6) Borrelli, N. F.; Hall, D. W.; Holland, H. J.; Smith, D. W. *J. Appl. Phys.* **1987**, *61*, 5399.
(7) Brus, L. E. *IEEE J. Quantum Electron.* **1986**, *QE−22*, 1909.
(8) Brus, L. E. *J. Phys. Chem.* **1986**, *90*, 2555.
(9) Brus, L. E. *J. Chem. Phys.* **1984**, *80*, 4403.
(10) Spanhel, L.; Haase, M.; Weller, H.; Henglein, A. *J. Am. Chem. Soc.* **1987**, *109*, 5649.
(11) Woggon, U.; Petri, W.; Dinger, A.; Petillon, S.; Hetterich, M.; Grun, M.; O'Donnell, K. P.; Kalt, H.; Klingshirn, C. *Phys. Rev. B* **1997**, *55* (3), 1364.
(12) Youn, H. C.; Baral, S.; Fendler, J. H. *J. Phys. Chem.* **1988**, *92* (22), 6320.
(13) Tian, Y.; Tewton, T.; Kotov, N. A.; Guldi, D. M.; Fendler, J. H. *J. Phys. Chem.* **1996**, *100*, 8927.
(14) Hines, M. A.; Guyot-Sionnest, P. *J. Phys. Chem.* **1996**, *100*, 468.
(15) Kortan, A. R.; Hull, R.; Opila, R. L.; Bawendi, M. G.; Steigerwald, M. L.; Carroll, P. J.; Brus, L. E. *J. Am. Chem. Soc.* **1990**, *112*, 1327.

(16) Mews, A.; Kadavanich, A. V.; Banin, U.; Alivisatos, A. P. *Phys. Rev. B* **1996**, *53* (20), 13242.
(17) Hässelbarth, A.; Echymüller, A.; Eichberger, R.; Giersig, M.; Mews, A.; Weller, H. *J. Phys. Chem.* **1993**, *97*, 5333.
(18) Spanhel, L.; Weller, H.; Henglein, A. *J. Am. Chem. Soc.* **1987**, *109*, 6632.
(19) Spanhel, L.; Henglein, A.; Weller, H. *Ber. Bunsen-Ges. Phys. Chem.* **1987**, *91*, 1359.
(20) Henglein, A.; Gutierrez, M.; Weller, H. *Ber. Bunsen-Ges. Phys. Chem.* **1989**, *93*, 593.
(21) Mews, A.; Echymüller, A.; Giersig, M.; Schooss, D.; Weller, H. *J. Phys. Chem.* **1994**, *98*, 934.
(22) Jaskólski, W.; Bryant, G. W. *Phys. Rev. B* **1998**, *57*, 4237.
(23) Echymüller, A.; Mews, A.; Weller, H. *Chem. Phys. Lett.* **1993**, *208* (1), 59.
(24) Schooss, D.; Mews, A.; Echymüller, A.; Weller, H. *Phys. Rev. B* **1994**, *49*, 17072.
(25) Nirmal, M.; Norris, D. J.; Kuno, M.; Bawendi, M. G.; Efros, Al. L.; Rosen, M. *Phys. Rev. Lett.* **1995**, *75*, 3728.
(26) Cardona, M. *J. Phys. Chem. Solids* **1963**, *24*, 1543.
(27) Sirenko, A. A.; Belitsky, V. I.; Ruf, T.; Cardona, M. *Phys. Rev. B* **1998**, *58*, 2077.
(28) Hopfield, J. J.; Tomas, D. J. *Phys. Rev. B* **1961**, *122*, 35.
(29) *Defect Electronics in Semiconductors*; Matare, H. F., Ed.; Wiley Interscience: New York, 1971.